42nd AIAA Thermophysics Conference
27 - 30 June 2011, Honolulu, Hawaii

AIAA 2011-3957

Proposed Analysis Process for Mars Science Laboratory Heat Shield Sensor Plug Flight Data

Todd White[*] and Ioana Cozmuta[†]
ERC Inc., Moffett Field, CA 94035, USA

Jose A. Santos[‡]
Sierra Lobo, Inc, P.O. Box 344, Moffett Field, CA 94035, USA

Bernard Laub[§]
NASA Ames Research Center, Moffett Field, CA 94035, USA

Milad Mahzari[**]
Georgia Institute of Technology, Atlanta, GA 30332, USA

The Mars Science Laboratory (MSL) mission is scheduled to enter the Martian atmosphere in August 2012. Aboard the heatshield is the MSL Entry Descent and Landing Instrumentation (MEDLI) system that includes a series of embedded sensor plugs to measure in-depth response of the thermal protection system (TPS). The general objectives of the MEDLI system are to assess the TPS performance and reconstruct the aerothermal environment experienced during entry. Some specific objectives, such as measuring TPS temperature, can be addressed with direct measurements. Other objectives, such as determining surface heating, must be inferred using measurements combined with analytical tools. This paper describes the specific objectives, the expected sensor responses to the entry environment based on aerothermal and material response simulations, and the reconstruction analysis process being developed for the flight data.

I. Nomenclature

α	=	angle of attack, *degrees*
β	=	angle of sideslip, *degrees*
ε	=	Surface emissivity
λ	=	Blowing correction
q	=	heat flux per unit area, W/cm^2
B'c	=	Non-dimensional char mass loss rate
C_H	=	Film coefficient
H_{rec}	=	Recovery enthalpy *J/kg*
P	=	Pressure, *Pa*
V	=	Velocity, *km/s*
R	=	Total recession, *cm*
L	=	Length of sensing wire, *cm*
R	=	Resistance of sensing wire, Ω
T	=	Temperature of sensing wire, *K*
t	=	Time, *seconds*

[*] Research Scientist, Aerothermodynamics Branch, AIAA Member.
[†] Senior Research Scientist, Aerothermodynamics Branch, AIAA Member
[‡] Mechanical Engineer, Thermophysics Facilities Branch, AIAA Member
[§] Senior Aerospace Engineer, Entry Systems and Vehicle Development Branch, AIAA Fellow
[**] Ph.D. Student, School of Aerospace Engineering, AIAA Member

Acronyms

CHIEF	=	CHanging Inputs for the Environment of FIAT
EMF	=	Electro-motive force
DPLR	=	Data Parallel Line Relaxation hypersonic CFD code
DAS	=	Data Analysis Strategy
FIAT	=	Fully Implicit Ablation and Temperature material response code
LAURA	=	Langley Aerothermodynamic Upwind Relaxation Algorithm
MEADS	=	Mars Entry Atmospheric Data System
MEDLI	=	MSL Entry, Descent, and Landing Instrumentation
MSL	=	Mars Science Laboratory
MISP	=	MEDLI Instrumented Sensor Plug
HEAT	=	Hollow aErothermal Ablation and Temperature Sensor
IMU	=	Inertial Measurement Unit
PICA	=	Phenolic Impregnated Carbon Ablator
PS	=	Payload Science
SSE	=	Support System Electronics
SST	=	Shear Stress Transport
SEB	=	Surface Energy Balance
TC	=	Thermocouple
TPS	=	Thermal Protection System

II. Introduction

THE Mars Science Laboratory (MSL) mission is scheduled to launch in late Fall 2011 and land on the Martian surface in August 2012. MSL will be the largest planetary entry vehicle, with an entry mass of 3400 kg, and a heatshield 4.5 meters in diameter. The heatshield has tiled Phenolic Impregnated Carbon Ablator (PICA)[1] for the thermal protection system (TPS) material. The MSL heatshield is expected to experience turbulent heating prior to peak heating. The predicted heating and shear stress are far greater than were experienced by Pathfinder or the Mars Exploration rovers. While the MSL heatshield[2,3] was being designed, a parallel effort was underway to install detailed pressure and temperature instruments onboard to improve understanding of the entry environment and PICA response.

Figure 1. Completed MSL heatshield and underside with MEDLI system installed.

This effort, the MSL Entry, Descent, and Landing Instrumentation (MEDLI) project, was tasked with designing, delivering, and installing an instrumentation package on the MSL flight heatshield[4] to help characterize the MSL aerodynamics, aerothermodynamic environments,[5] and thermal protection system response during entry. The resulting MEDLI system consists of a data acquisition system, pressure transducers, and in-depth temperature sensors embedded in the TPS. Figure 1 shows the outside and underside of the MSL heatshield. The underside view has the pressure transducers and harness clearly visible. As of publication, the MEDLI system has been successfully installed on the MSL heatshield.

MEDLI's pressure transducers are part of MEADS (Mars Entry Atmospheric Data System) and the temperature measuring thermocouple and isotherm sensors make up the MISP (MEDLI Integrated Sensor Plug) system. This paper focuses on the MISP system; MISP and MEADS heatshield locations are shown in Figure 2.

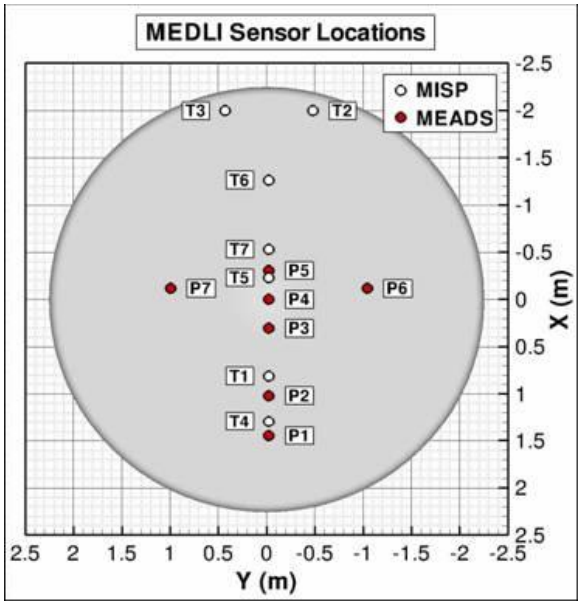

Figure 2. Locations of the MEADS and MISP system.

Each MISP contains four in-depth thermocouples (TCs) and one isotherm tracking Hollow aErothermal Ablation and Temperature (HEAT) sensor.[6] In order to improve characterization of the MSL entry environment and TPS response, the MISP system was designed to directly inform certain aspects of re-entry physics and material performance. First, at each MISP location, TCs and HEAT sensor data will be recorded, thereby providing local TPS temperature histories that will be used to assess how well the TPS performs.

Second, using the direct measurements of each MISP, it should be possible to assess the surface aerothermal entry environments to which the TPS is subjected. For each plug, this will require solution of an inverse problem employing a computational model for PICA. These reconstructed environments should capture effects such as turbulent heating, transition, and gas-surface interaction that are of paramount importance in vehicle design. More broadly, we expect to gain an understanding of how the heatshield as a system performed, and what the distributed aerothermal environments must have been on the vehicle during entry.

MEDLI builds on a long history of ablative heatshield instrumentation, including Pioneer Venus,[7] Galileo,[8] and Mars Pathfinder.[9] The combination of MISP and MEADS instruments will produce the largest flight dataset for planetary entry to date; the number of heatshield thermocouples alone is four times greater than that flown on Mars Pathfinder.

While the actuality of extensive MSL heatshield instrumentation is exciting for the aerothermal and material modeling communities, indications are that reliable MEDLI data reduction presents several challenges. The following sections will discuss the specifics of the science requirements and the analysis tools and techniques being used. They cover the expected MISP system response to Martian entry, and outline the authors' proposed iterative processes for analyzing the MISP flight data.

III. Science Objectives and Simulated MISP Response

The MEDLI project science requirements specify the objectives and desired accuracy of measurements to be made using the MISP system. The seven payload science (PS) requirements (PS-363-369) are summarized below, in Table 1.

Table 1. MISP Payload Requirements Mapping

Level 2 Requirement	Objective	Accuracy	T1	T2 & T3	T4	T5	T6	T7
PS-363	Reconstruct basic and stagnation point aeroheating	± 30 W/cm^2	X	X	X	X	X	X
PS-364	Determine leeside turbulent heating levels	± 30 W/cm^2		X		X	X	X
PS-365	Measure depth of isotherm in TPS	720^{o}C ± 80^{o}C and ± 0.8mm	X	X	X	X	X	X
PS-366	Determine if any windside heating augmentation occurs	± 30 W/cm^2	X		X	X		
PS-367	Determine total TPS recession	± 0.635 cm (0.25 in)		X		X	X	X
PS-368	Measure subsurface material temperature response	± 12%	X	X	X	X	X	X
PS-369	Determine time of turbulent transition	2 seconds		X		X	X	X

Table 1 highlights which MISP sensors in combination will be used to address each science objective. The selection of these sensors is driven by their location on the heatshield. For instance, those MISPs expected to experience discernible turbulent augmentation (T2, T3, T5, T6, T7) are relevant to PS-364 and PS-369. Plugs near where windside augmentation may occur (T1, T4, and T5) are relevant to PS-366. Other objectives will need data from all of the plugs to meet the requirements.

The contents of Table 1 represent the most up-to-date requirements for MISP as of publication, and include changes from those presented previously.[5] These changes were mostly in requirements accuracy, from relative to absolute values. However, there have been more substantive changes to PS-365 and PS-367 made by the MEDLI project. In particular, an earlier recession rate objective (formerly PS-365) was changed to a requirement for measuring an isotherm depth. This change was due to uncertainty in the HEAT calibration data used to correlate isotherm rate and recession rate across the wide range of conditions expected at each plug; reference 10 describes ongoing laboratory and arc-jet tests to improve the HEAT sensor calibration. The accuracy of PS-367 (total TPS recession) was changed to reflect usage of the thermocouple burn-throughs for recession determination, rather than the integrated recession rate specified with the old PS-366 requirement.

The aerothermal and material response quantities of interest, including heat flux and surface recession, are not directly measured and must be inferred from the measured in-depth TPS temperatures and isotherm time histories. Thus only PS-365, PS-366, and PS-368 can be addressed through direct measurement. The remaining objectives (PS-363, PS-364, and PS-369) need reconstruction and data analysis informed by both computational fluid dynamics (CFD) and material response simulations.

For the original MSL vehicle design,[5] the Langley Aerothermodynamic Upwind Relaxation Algorithm (LAURA)[11] and Data Parallel Line Relaxation (DPLR)[12] real-gas Navier-Stokes flow solvers were used to derive the MSL aerothermodynamic environments. For this paper, the MSL heatshield is simulated using the DPLR code V4-02-1. DPLR is a modern, parallel, structured non-equilibrium Navier-Stokes flow solver maintained at NASA Ames Research Center. The code employs modified Steger-Warming flux-splitting scheme, for higher-order differencing of the inviscid fluxes.

The flow over the heatshield is modeled as being in a state of thermochemical non-equilibrium, using the Mitcheltree and Gnoffo 8-species 12-reactions Mars atmosphere (CO_2, CO, N_2, O_2, NO, C, N, O).[13] The TPS surface is modeled as non-slip radiative equilibrium wall with constant emissivity and a range of surface catalycity models. Turbulence and transition are simulated using both Baldwin-Lomax[14] turbulence models and Menter's shear stress transport (SST) vorticity-based turbulence model.[15] Radiative heating was considered to be negligible during vehicle design, but may be included in future analysis using the NEQAIR code.[16] Thus far, bank-angle effects have been neglected ($\beta = 0$) to exploit symmetry and reduce CFD calculation time, but will be included in follow-on analysis.

The MSL program also developed a comprehensive bias and margins policy for the heatshield sizing, which was performed with the Fully Implicit Ablation and Thermal (FIAT)[17] response code. FIAT is a material response code that solves the one-dimensional time-accurate equations of thermal diffusion with surface ablation and internal pyrolysis. FIAT solves two types of equations, the first is in inside the solid where FIAT models phase change reactions from virgin solid to charred solid and pyrolysis gas using measurements of macroscale properties and thermodynamics from the NIST/JANAF database. The second is at the surface, where FIAT solves for a complex surface energy balance (SEB) that accounts for thermochemical ablation and boundary layer heat transfer with blowing corrections. For this analysis the PICA[18] material response is modeled using the FIAT v2.5.1 code with the same PICA model and substructure materials as was used for the MSL TPS design.

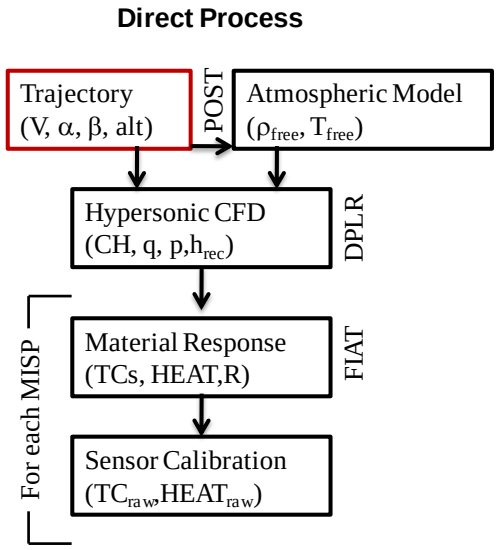

Figure 3. Direct analysis process for predicting MISP response.

We simulate MISP environments using a combination of DPLR steady-state simulations along the anticipated MSL entry, followed by material response simulations based on those CFD results at each MISP location (Figure 3). This prediction procedure contains the following steps:

1) Begin with known (or simulated) vehicle trajectory data (α, β, altitude, T, V) used as inputs to DPLR. Based on a Mars atmospheric model (i.e. *MARSgram*), altitude and temperature are mapped to atmospheric density.
2) Density and vehicle trajectory data are used as boundary conditions for a series of steady-state simulations of the MSL forebody. These simulations may be 1-10 seconds apart from each other, and cover the convective heating and pressure pulse. An example is shown in Figure 4 for MISP T2, along with the input trajectory.
3) CFD simulations are post-processed to extract computed surface pressure, heat flux, surface enthalpy, boundary layer edge enthalpy, and shear stress. Each of these time histories is interpolated with a monotonic cubic spline curve in time to 0.1 second intervals. These outputs are gathered for every plug location.
4) FIAT material response simulations are run at the MISP locations to compute thermocouple temperature, isotherm, and in-depth material properties as a function of time. These results can now be compared to post-processed MISP sensor data.

Each analysis step involves model selections that must be consistently applied throughout the simulation process. For instance, after step 4, material response will predict a surface temperature and emissivity that can be used to correct the CFD simulations, and iterated to convergence.

We next discuss how each of the previously mentioned science requirements is addressed using sensor calibration and the described DPLR and FIAT analysis tools.

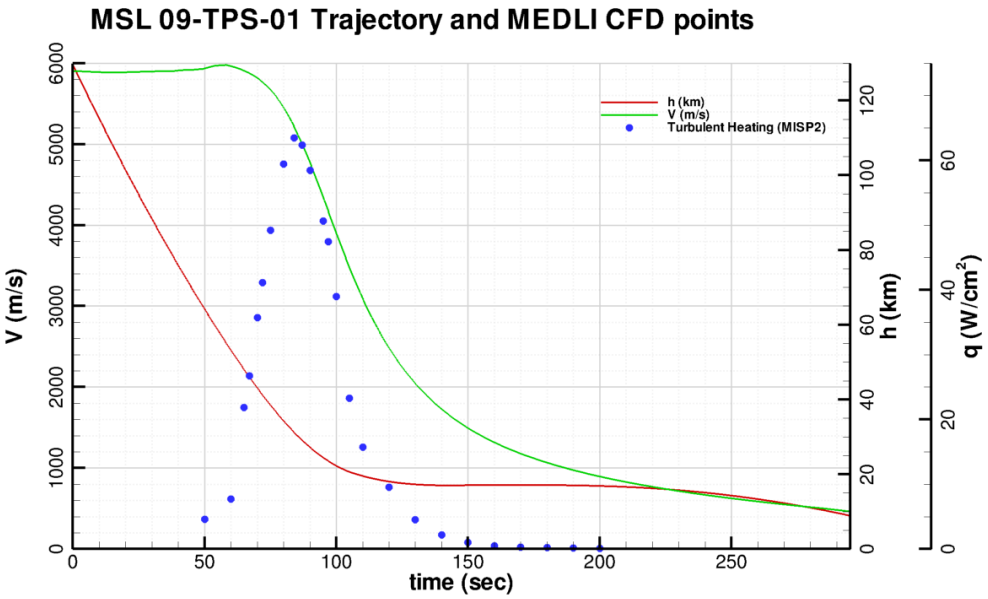

Figure 4. MSL trajectory and heating at MISP T2.

B. PS-368 Subsurface Material Response

The PS-368 requirement reads: *Measure temperature response of the TPS, ± 12%, as a function of time from entry interface at multiple depths at seven locations on the heat shield*. This requirement is directly tied to the installed thermocouples in each plug, shown in Figure 5. Each MISP consists of four type-K thermocouples in a PICA cylinder 3.3 cm diameter by 2.9 cm long. The two near-surface thermocouples (at 0.254 cm and 0.508 cm depths respectively) are sampled at 8 Hz, while the two deeper TCs (1.143 cm and 1.778 cm depths) are sampled at 1 Hz. The thermocouples, which experience an electro-motive force (EMF) based on temperature changes, are connected to the Support System Electronics (SSE) box.[5]

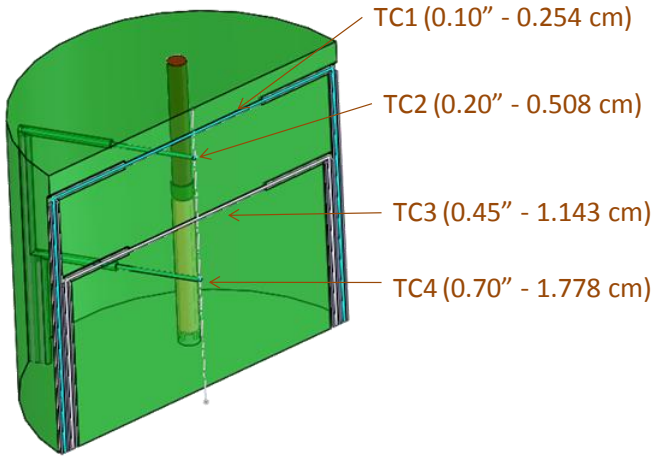

Figure 5. MISP plug cross section.

The electro-motive force (EMF) is quantified by measuring the electric potential (voltage) difference between the hot and cold junctions of each MISP thermocouple. A 9th-order polynomial published by NIST based on the ITS-90 standard is used to convert the EMF signal to temperature. The thermocouples are Type K, consisting of Chromel and Alumel metal with a 0.31-mm (0.012-in) diameter bead hot junction. The required measurement range is 100 – 1300 Kelvin. Although the SSE will record EMF output corresponding to temperatures above 1300 K (up to the

1673 K temperature at which the Alumel wire begins to melt), the data in this range are considered unreliable for post-flight data analysis. This is because the interaction of the Chromel and Alumel wires with the TPS material at high temperatures is not well characterized, and the calibration of the thermocouples does not extend to this high temperature range.

A two-dimensional finite element analysis with specified surface temperature and surface velocity boundary conditions was completed for the MEDLI project to study the thermal lag associated with the installation of the MISP thermocouples. The analysis was based solely on heat conduction (no internal decomposition) using virgin properties of PICA. Figure 6 plots the worst-case time lag as a function of temperature for the MISP T2 location on the heat shield. The MISP error budget document[19] details the individual sources of errors, and overall each TC is expected to meet the requirement of temperature prediction within ±12% for the 100-1300K range.

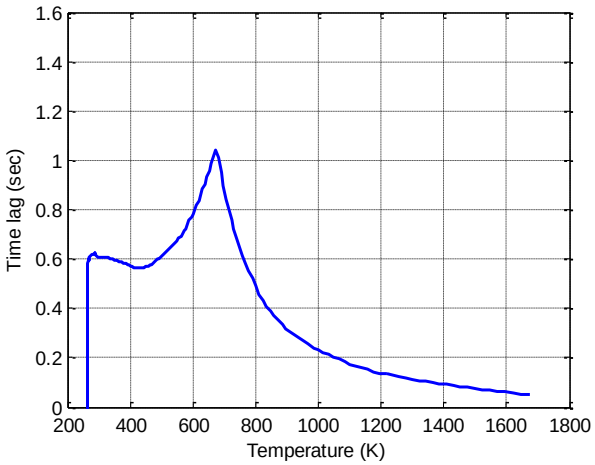

Figure 6. Finite element analysis prediction of the worst-case thermocouple lag.

Although it is difficult to predict anomalies that may occur in the flight data, based on ground tests it is expected that relatively little post-processing of the raw thermocouple signal will be required. This is due in large part to the built-in signal conditioning and fault-tolerance features of the SSE.[20] The main raw data post processing activity expected will be converting voltage to temperature and qualitatively examining the data above 1300 K. The onset of an open circuit between 1300 and 1673 K, for instance, will suggest thermocouple burn-through.

C. PS-367 Total TPS Recession

This requirement reads: *Determine the total integrated TPS recession, ± 0.25 inches (0.635 cm), at each MISP location.* Based purely on the sensor overtemping, burn-through and corresponding signal loss, we can estimate TPS recession as a step function based on the discrete TC depths. Using the conservative MSL design environments, MISP T2 and T3 may experience severe enough environments for the surface to recess past the top three thermocouples. Additionally, the predicted isotherm depth from the HEAT sensor can also be interpreted simply as a bound on the surface recession. Using just the TCs, we expect to meet the TPS recession requirement above, within ± 0.25 in, or better if the final recessed surface falls between the shallower TCs.

Though the best way to determine recession is when a near-surface thermocouple burns out when the surface approaches its depth, we also consider estimating surface recession using the results predicted from FIAT at each plug. This is possible if the actual flight sensor data can be reconciled with FIAT outputs, as described later in Section IV. A study has been conducted with FIAT to evaluate the sensitivity of the response of the in-depth thermocouples in the MISP plug to uncertainties in surface recession. For this purpose, the focus was on the response of MISP T2 where maximum heating and recession are anticipated. The non-dimensional char mass loss rate (B'c) was augmented by 25, 50 and 100% in comparison to nominal without modifying any terms in the surface energy balance. Limitations in the recession augmentation in FIAT meant only artificially *in*creased recession could be studied. Figure 7 illustrates how surface recession scales with B'c. The figure also shows that the predicted surface temperature is relatively insensitive to the surface recession, which is not surprising since the augmentation does not change the SEB energy terms.

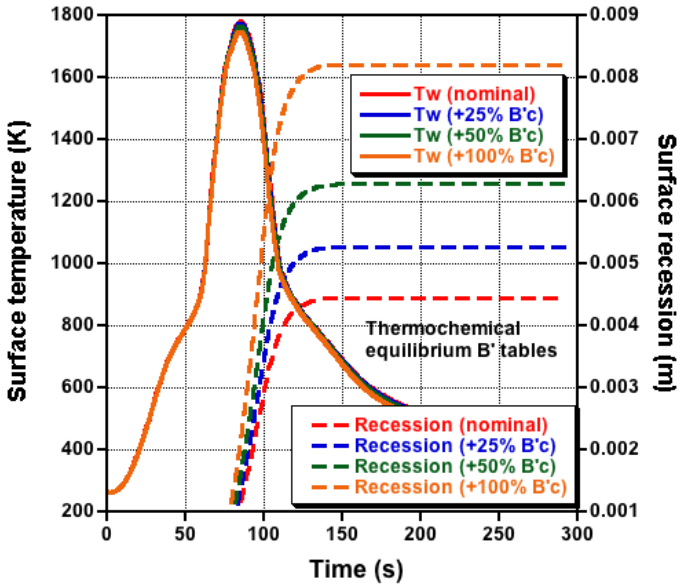

Figure 7. Sensitivity of recession and surface temperature to B'c.

Figure 8 illustrates the predicted time-dependent temperature response at the nominal depths of the thermocouples in the MISP T2 plug. As seen, the TC at a depth of 0.261 cm is predicted to burn-through even at nominal heating. However, the thermocouple at a depth of 0.491 cm is predicted to burn-through only if surface recession is 50-100% greater than nominal. Furthermore, as shown in Figure 8, the thermal response of these TCs is relatively insensitive to model uncertainties in recession. Thus it will be challenging to use the existing material model to predict surface recession more accurately than just using only TC burn-through.

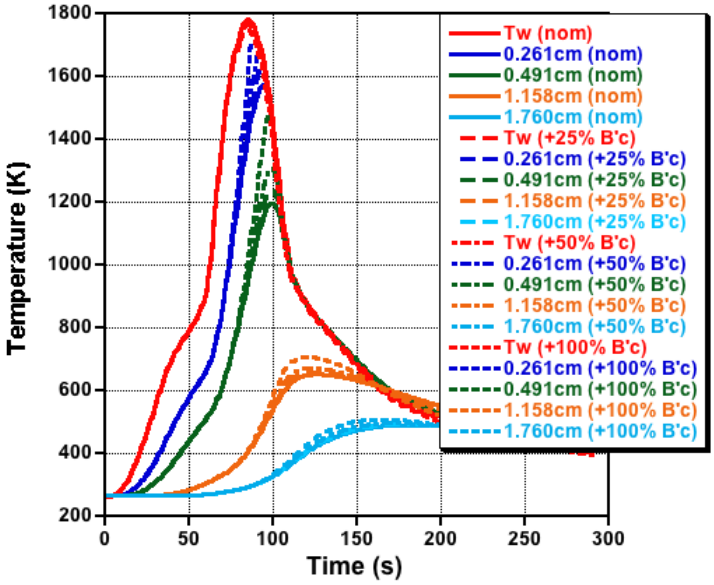

Figure 8. Sensitivity of in-depth temperatures to uncertainty in recession.

D. PS-365 TPS Isotherm Depth

The payload science requirement is: *Measure the depth of a 720°C ± 80°C isotherm to within ±0.8mm, as a function of time from entry interface at multiple locations on the heat shield*. This requirement is met through a calibrated response from each of the seven HEAT sensors in each MISP plug. The HEAT sensor[6] consists of wound Tungsten wires in Kapton tubing. The tubing becomes electrically conductive when charred and changes the resistivity of the wound wires. All HEAT sensors are sampled at 8 Hz.

The SSE provides a 1 mA constant current source excitation to each HEAT sensor, which enables the voltage drop across the lead wires of the HEAT to be measured (see Figure 9). The voltage reading is related to the resistance of the two wound Pt-W wires in series with the current source simply via Ohm's law. The resistance determined from the voltage measurement is proportional to the sensing length *L(t)*.

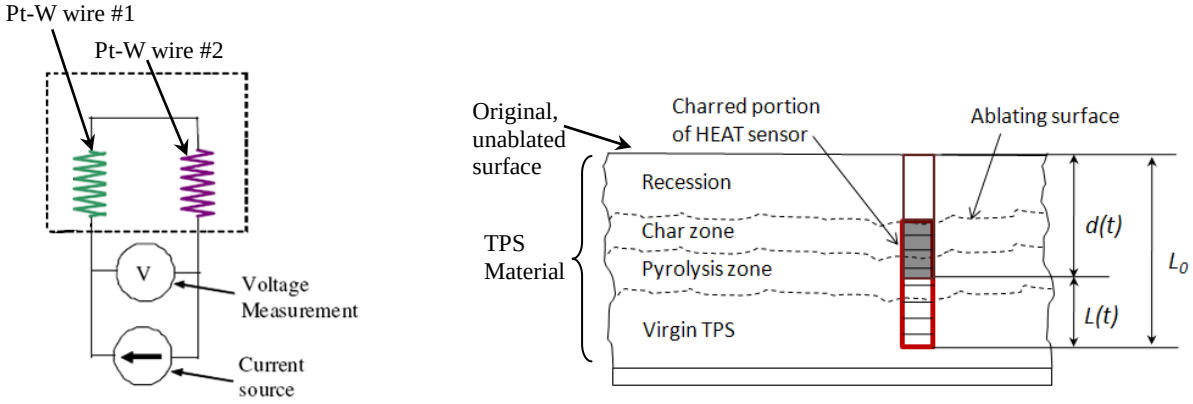

(a) HEAT sensor equivalent circuit

(b) HEAT sensor output *L(t)*.

Figure 9. HEAT sensor electrical circuit and measurement output.

Though it is often called a "recession sensor," the HEAT only tracks an isotherm through the material. For the case of steady-state ablation, where the surface is recessing at the same rate as char is being created, the recession rate and HEAT measured rates are equal. This requires the surface heating conditions to be relatively constant, at least on the order of seconds. However, for the expected heating pulse on MSL, the surface conditions are expected to change too rapidly for the material to be in steady-state ablation.

Initial findings from laboratory experiments indicate the isotherm temperature tracked by the HEAT sensor is dependent on the temperature ramp rate, *dT/dt* of the Kapton. For a ramp rate of 450 °C/min, the isotherm temperature is predicted to be 720°C ± 60°C. Reference 10 discusses the HEAT sensor calibration in greater detail.

E. PS-363 Basic and Stagnation Point Aeroheating

The payload science requirement is: *Reconstruct a basic distribution of heating levels, ± 30 W/cm^2, as a function of time from entry interface at seven locations on the aeroshell, including the flow stagnation point, from near-surface temperature and isotherm measurements.* To assess this requirement we must investigate the sensitivity of the MISP instruments to surface heating.

The magnitude of predicted convective heating[5] is highly dependent on model selection, in particular surface catalycity and turbulence modeling. Maximum heating occurs near the leeward shoulder point at 84 seconds from entry interface using the MSL TPS 09-01 trajectory. In the benign case, the peak heating is less than 80 W/cm^2, and in the most conservative design scenario, 220 W/cm^2.

Using the DPLR process described earlier, we start with the time-varying heat flux profile at each MISP location and a range of predicted heating pulses for each. To determine the expected worst-case sensitivity of each MISP to surface heating, we linearly scale the convective heating pulse at each plug and simulate the plug response to the scaled and original environments. The scaled environment that results in a TC deviating beyond the absolute measurement uncertainty (± 12%) is used to determine the MISP instrument sensitivity (Figure 10).

Each plotted point represents the result of many FIAT simulations along five separate heat pulses. The data are each plotted by the heat pulse peak, and a bounding curve fit is also shown (blue line). One can interpret the data to mean that a MISP exposed to a simulated MSL heat pulse that peaks at 140 W/cm^2 has a worst-case uncertainty in the heating profile of ± 20 W/cm^2. Using these simulations and material model it appears the ±30 W/cm^2 requirement is achievable.

Interestingly, the apparent TC measurement uncertainty in heat flux drops off for both more extreme and more benign entry environments. But the relative error is compounded at these benign conditions. If plug T1 experiences a heating pulse with peak of only 25 W/cm^2, the MISP plug is sensitive only to ± 7 W/cm^2, almost a 50% uncertainty. Fortunately, using improved models of the thermocouples including separating the sensor uncertainties into relative lags, biases, and random noise may increase the TC sensitivity to surface heating.[19]

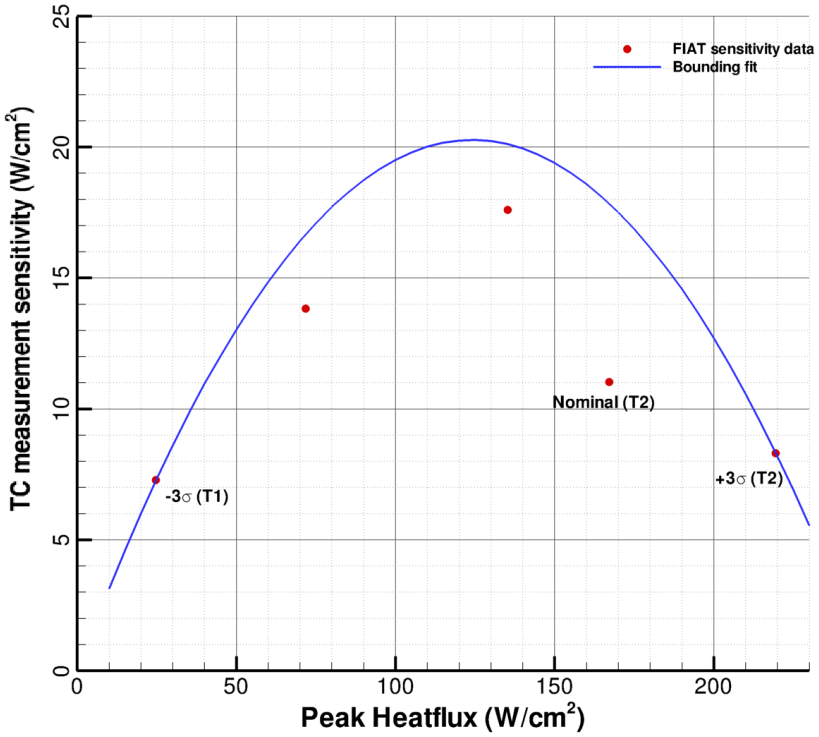

Figure 10. Simulated TC sensitivity of PICA FIAT model to scaled heat flux.

F. PS-364 Turbulent Leeside Heating Levels and PS-369 Turbulent Transition

The payload science requirement is: *Determine the turbulent heating level on the leeside of the heat shield, ± 30 W/cm^2, as a function of time from entry interface at multiple locations, including the geometric apex and the predicted peak turbulent heating location from near-surface temperature and isotherm measurements.* Also for time of turbulent transition, the requirement is: *determine the time at which the flow field transitions from laminar to turbulent at multiple locations on the heat shield to within 2.0 seconds, from near-surface temperature and isotherm measurements.*

To simulate the expected effect of turbulence, we use the models available in DPLR. As discussed earlier, DPLR has Menter's SST turbulence model, as well as the Baldwin-Lomax model, which in DPLR can be tuned at the surface with great control. Laminar, SST, fully turbulent Baldwin-Lomax, and Baldwin-Lomax with transition are used to simulate surface heating at all MISP locations. The resulting environments are plotted in Figure 11, with a side-by-side comparison of laminar and Baldwin-Lomax turbulent heating, as well as centerline comparisons with more models. The solid red line (fully turbulent from the stagnation point) is the most conservative, and is the assumption used for vehicle design. The red-dashed line (Baldwin-Lomax with transition) and purple line (Menter's SST model) are believed to be more physically realistic, and enforce natural transition on the surface. The transitioning Baldwin-Lomax solutions employ a criterion of Reynolds number based on boundary layer momentum thickness (Re_θ). This Re_θ criterion is computed in the laminar solution (green line), and the Baldwin-Lomax model is fully laminar at $Re_\theta \leq 150$ and fully turbulent at $Re_\theta \geq 250$.

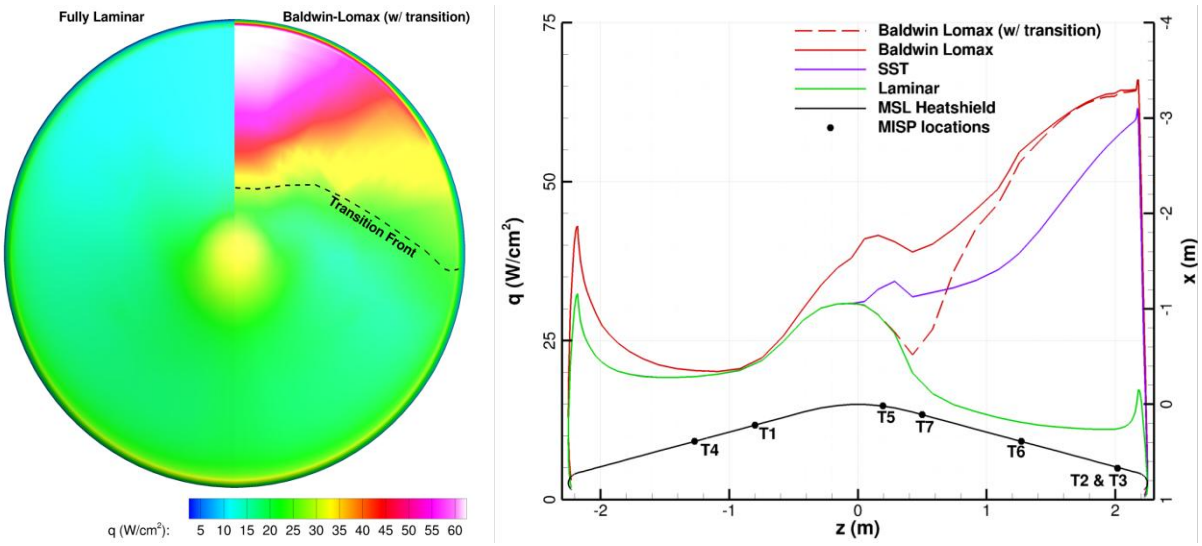

Figure 11. CFD predicted MSL laminar and turbulent environment at t = 84.

In simulations, we can control the onset and extent of turbulent heating augmentation, but in the flight reconstruction it must be estimated using the in-depth TCs. We expect that transition will be marked with a rapid rise in temperature at near-surface thermocouples and an increase in speed of the HEAT sensor rate. To this end, aerothermal environments generated with laminar and turbulent assumptions are applied to each MISP plug.

Figure 12 demonstrates the effect of turbulent heating augmentation on simulated sensor response for MISP T2 and MISP T7. For MISP T2, TC response based on fully laminar environments (dashed lines) match the transitional Baldwin-Lomax (solid lines) at first. Just after turbulent transition (~60 seconds), there is a sudden slope change in the near surface TCs, with the shallowest TC responding most quickly. For MISP T2 the increased heating is severe enough to burn-through the top TC. It is expected that any such pronounced response means part of the science requirements can be met, namely augmentation within ± 30 W/cm^2. Additional simulations and arc-jet tests are planned to demonstrate that the requirement can be met across the range of possible environments; further study is needed to verify time of transition can be identified within 2 seconds.

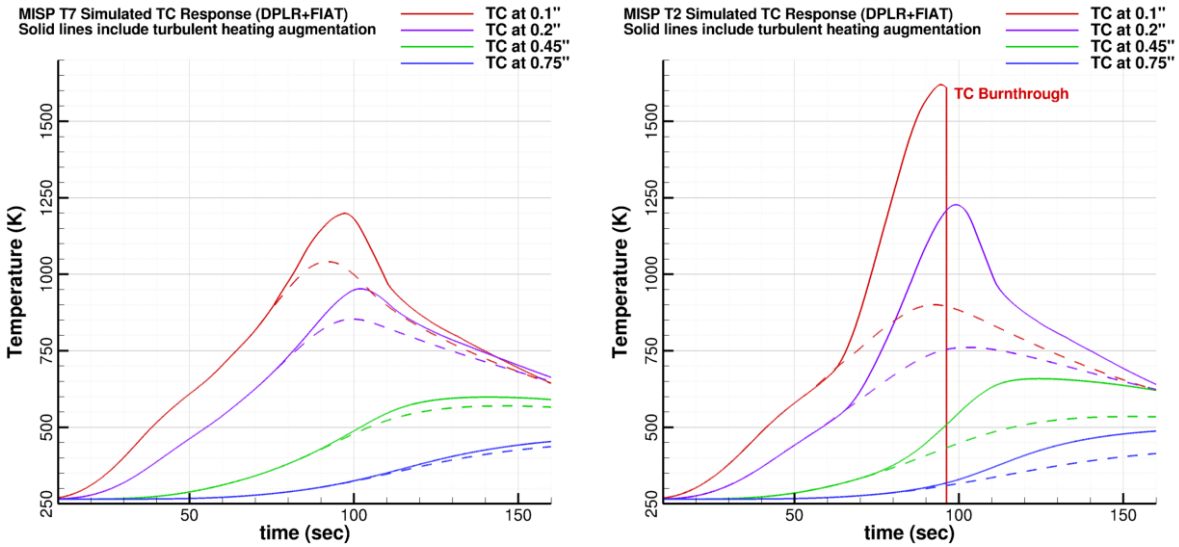

Figure 12. Response of MISP T7 and T2 to laminar and turbulent environments.

G. PS-366 Windside Heating Augmentation Levels

The payload science requirement reads: *Determine whether augmented heating, > 30W/cm^2 above nominal laminar levels, occurs in the flow stagnation region, as a function of time from entry interface from near-surface temperature measurements and isotherm measurements.*

This objective is much like the turbulent heating payload science requirement, where we must detect whether there is augmented heating in a particular region. The windside heating phenomenon, seen experimentally in AEDC T9,[21] may lead to elevated heating levels of up to 50% near the stagnation point. Figure 13 shows increased heating in the windside region (-1.0 > x/R > -0.2). In wind-tunnel testing, this phenomenon occurs in a specific range of freestream Reynolds numbers. Therefore, if it appears in flight, it is expected to occur during a portion of the heating profile, rather than for the entire pulse.

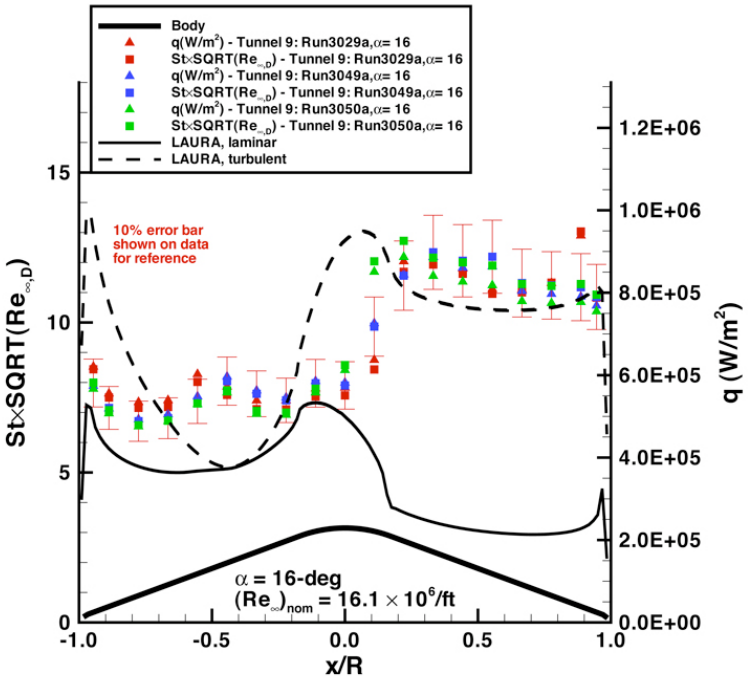

Figure 13. Windside heating at Mach 8 in AEDC Tunnel 9 MSL tests.[21]

To simulate the response of the MISP sensor to this phenomenon, MISP plug T1 is subjected to gradual 20% heating augmentation prior to vehicle peak heating (at 70 seconds). The resulting impact on the simulated MISP plug is shown in Figure 14 below. As with the turbulent augmentation, there is a detectable deviation in the in-depth temperatures depending on the absence or presence of windside augmentation. At near-surface TCs the effect of heating augmentation is visible in the TC slope and peak temperature, while in the deeper TCs the effect is less pronounced and lags. As with turbulent augmentation, we anticipate being able to meet this requirement, and detect the presence of windside augmentation if is above 30 W/cm^2.

This concludes the discussion of each individual science requirement, and we will now discuss the overall proposed analysis process.

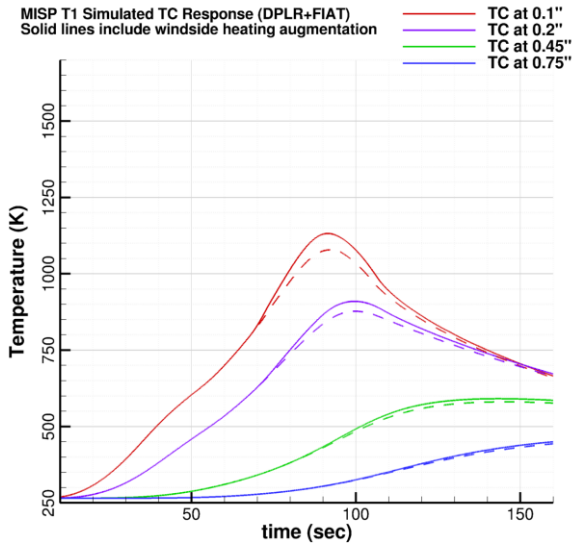

Figure 14. Response of MISP T1 to simulated windside heating augmentation.

IV. Proposed Analysis Process for MISP Flight Data

The main focus of the MISP post-flight analysis is to ensure that the payload science objectives are met, so to fully exploit the flight data, a data analysis strategy (DAS) is being assembled. The DAS represents a plan for using the flight data from each MISP to address the science objectives.

The MEDLI system will be turned on and gathering data ten minutes prior to entry, thus the first use of flight data is to established that the instrumentation itself functions properly, based on the presence of signals for each sensor in each plug. Next, by comparing the signals received at the seven MISP locations (for all TCs and HEAT sensors) an estimate of the signal to noise (S/N) ratio in constant environments will be obtained. The S/N ratio will then be reevaluated for all the locations/depths under thermal environments in the first few seconds during entry. To best exploit the flight data set, the DAS should build upon the fact that the uncertainty in relative heating at any two MISP locations is lower than the absolute uncertainty corresponding to any individual MISP. For example, should a given ratio between two MISP locations drastically change, it is likely due to either a physical phenomenon such as transition to turbulence or to a hardware error. If this is due to a physical phenomenon, it should propagate in depth and be observed at deeper TCs while a hardware error should remain isolated.

After the above consistency check on the sensor data, a comparison will be made with the predicted sensor response (using CFD and material response simulations described earlier). Given the wide range of possible environments that MSL may experience, and inherent material modeling uncertainties, a method for reconciling predictions and measurements is a necessity. Figure 15 shows a modified form of the Direct Analysis strategy presented earlier, with two iterative loops shown. These loops are in development, and at the time of writing it is hoped they will be used to reconcile the predicted environments with those measured in flight.

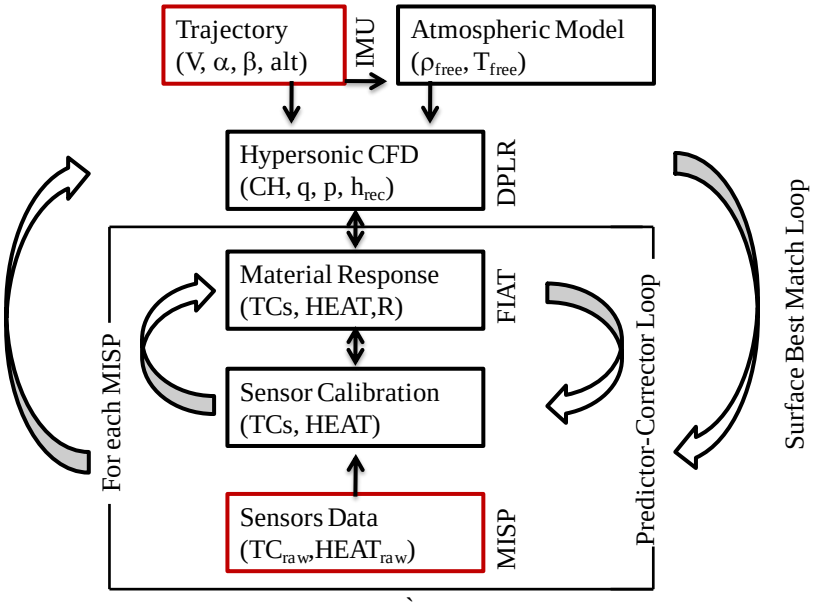

Figure 15. Proposed Data Analysis Strategy.

A. Predictor-Corrector

We are developing two separate predictor-corrector loops as part of the DAS, the first operating locally at each MISP plug. This loop is used iteratively to match simulated TC data and isotherms to the calibrated sensor data output by adjusting the input aerothermal environment. Currently all thermocouples are weighted equally, based on a least-squares best match between FIAT output and the calibrated target sensor data. An example of an existing Predictor-Corrector loop, called CHIEF,[22] is shown applied to a TC dataset from a constant condition arc-jet test. In Figure 16, CHIEF was provided the TC dataset and a starting guess of the test conditions. CHIEF iteratively changed the test conditions in FIAT (edge enthalpy, surface pressure, and film-coefficient) until it reached the best match, also shown in Figure 16, with FIAT-predicted TC responses co-plotted with actual sensor data.

The CHIEF code converges for constant surface conditions (such as in an arc-jet), however, CHIEF struggles with flight-like heat pulses experienced in entry scenarios. This has prompted development of more stable and better-controlled iterative methods. There are ongoing efforts at NASA Ames to reconstruct surface environments with in-depth material response by using loosely coupled least-squares time history matching techniques. Alternate techniques, employing future time methodology,[23] are in progress at Johnson Spaceflight Center for Orion Flight Test 1.

The Predictor-Corrector method should provide a means to reconstruct a surface profile of at the film coefficient (C_H) at each MISP location, as well as a corresponding surface heat flux profile from their in-depth temperature history. Additionally, biases and defects in the sensor data can be simulated, to assess the impact on the surface heating reconstruction. These methods require a starting guess of the time-varying material response inputs (H_{rec}, P, CH, and λ) that come from CFD calculations.

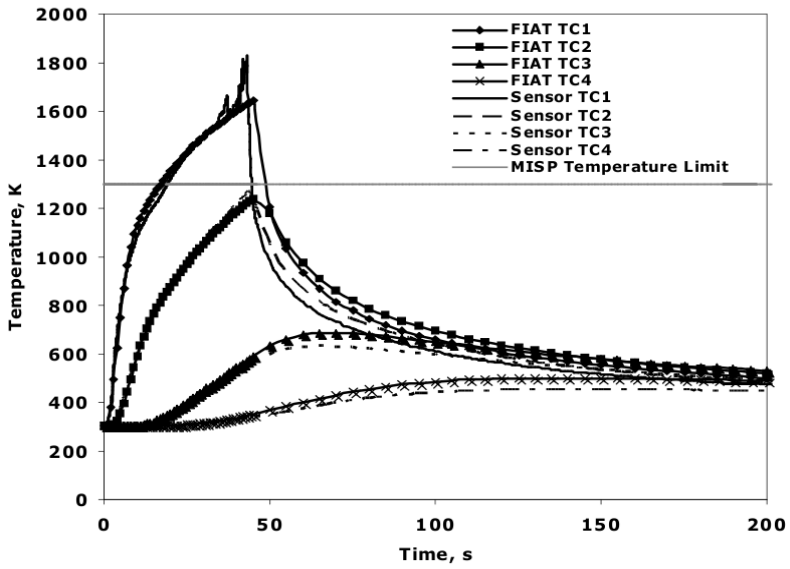

Figure 16. CHIEF/FIAT simulated thermocouples and actual arc-jet TC data.

B. Distributed Surface Best Match

This process attempts to match surface heating history globally, at all MISP locations. Here the focus is on how expected surface flow phenomena result in deviations in the shape of the predicted C_H/heating profile, such as the width and shape of the heat-pulse, slope changes, and peak heating values shown in Figure 17. With a heating profile reconstructed at each of the plug locations, global surface heating trends can be inferred based on differences between the plugs.

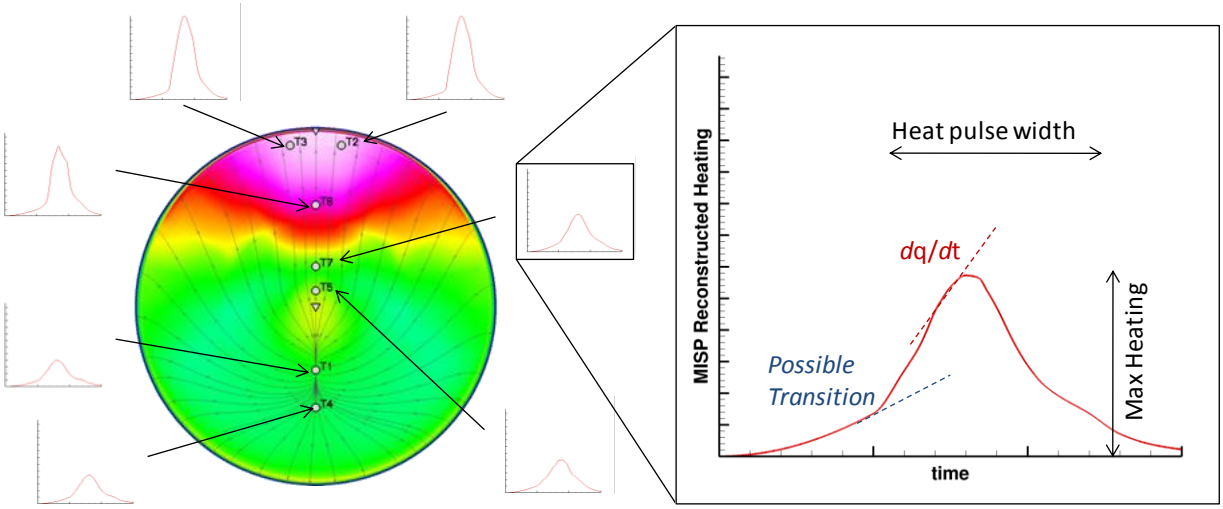

Figure 17. Using MISP distributed reconstructed profiles to infer global trends.

For example, at each of the steady-state CFD simulations, we can build sensitivity matrices of the aerothermal output parameters to describe their influence on simulated sensor response. As shown in Section III, turbulent heating augmentation should lead to a readily discernible slope change in the heat flux profile for some plugs. We generally expect a turbulent transition front to move from plugs MISP T2 & T3, to MISP T7, and further towards the sphere cone interface to MISP 6.

Prior to the return of MSL flight data, the techniques to reconstruct surface trends will primarily be applied to simulated flight data, though they may also be applied to other entry vehicle instrumentation and arc-jet test data.

The framework to apply the data analysis strategy discussed here is in development as of the publication of this paper, and is being tested using the sample environments and studies discussed in Section IV.

C. Limitations of Proposed Analysis Methods

Any design or reconstruction analysis is limited by the accuracy, applicability, and traceability-to-flight of the computational models employed. For instance, the current PICA model is applicable and demonstrated at high heat flux conditions, where the FIAT equilibrium surface chemistry model is appropriate. We are studying the impact to the MISP reconstruction of the model accuracy at lower heating regimes (where equilibrium may be inappropriate).

The approach outlined thus far attempts to decouple the material response aspects from the reacting flow imposed at the TPS surface. The separation of sensor calibration, material response, and computation fluid dynamics analysis is convenient and mirrors design practices. Two further efforts are ongoing to help integrate these distinct analyses; one is to develop a comprehensive parallel inverse parameter estimation strategy.[24] The other is to more tightly couple of the computational tools, DPLR and FIAT. In particular, we are investigating a finite rate surface chemistry performed in DPLR, instead of assuming the gas-surface interaction can be modeled with a simplified set of catalytic reactions.

The sheer volume of data collected by the MISP sensors means the reconstruction strategy should be automated whenever feasible. The ability to perform analysis quickly and consistently is critical, whether to use updated trajectories (such as the flight IMU reconstruction), to perform sensitivities on sensor degradation, or to directly address the science objectives.

V. Conclusions and Future Work

The primary forward work is to mature the data analysis strategy, in particular the predictor-corrector and best surface match scheme. It has already been determined that we will need to reduce uncertainty in the existing PICA material models with additional material properties testing. We anticipate this reconstruction preparation and activity after entry may highlight necessary improvements in ablator modeling and real-gas CFD.

In addition to the analysis and development discussed above, there is an ongoing arc-jet test campaign towards HEAT calibration. The MISP plugs were qualified and tested primarily at constant MSL design conditions, thus it is necessary to verify the MISP response to lower heating conditions, as well as transient heat pulses more representative of flight. This may be done by changing arc-jet flow conditions during tests, or with a rotating or arc-jet model. Additionally, these arc-jet tests are expected to provide further data not available for MSL entry: pyrometers and infrared cameras will provide surface temperatures, and photogrammetric recession can be used to determine surface recession profile with time.

The data returned from MSL will be the single largest dataset from any planetary probe heatshield. This information will be usable in the short-term for the TPS response and aerothermal reconstruction. However, the MISP sensor information will be available for future analysis and Mars programs; ideally it will be used to reduce design uncertainties. It is hoped that the experience and techniques developed here are applicable to future instrumented heatshields.

Acknowledgments

This work is funded in part by NASA Aeronautics Research Mission Directorate (ARMD) for MEDLI post-flight analysis efforts, as well as the ESMD for hardware, testing of installed flight hardware. Portions of this work were completed under contract NNA10DE12C to ERC, Inc and NNA09DB39C to Jacobs Engineering.

References

[1]Tran, H., et al., "Phenolic Impregnated Carbon Ablators (PICA) as Thermal Protection Systems for Discovery Missions," NASA TM-110440, April 1997.

[2]Beck, R.A.S., et al., "Development of the Mars Science Laboratory Heatshield Thermal Protection System," AIAA Paper 2009-4229, June 2009.

[3]Wright, M., et. al, "Sizing and Margins Assessment of the Mars Science Laboratory Aeroshell Thermal Protection System" AIAA Paper No. 2009-4231, June 2009.

[4]Gazarik, M., et. al, "Overview of the MEDLI Project," IEEE Paper 2008-1510, IEEE Aerospace Conference, Big Sky, MT, March 2008.

[5]Edquist, K., et. al, "Aerothermodynamic Design of the Mars Science Laboratory Heatshield", AIAA Paper No. 2009-4075, June 2009.

[6]Oishi, T., Martinez, E., and Santos, J., "Development and Application of a TPS Recession Sensor for Flight,"AIAA Paper No. AIAA 2008-1219, Jan. 2008.
[7]Wakefield, R., Pitts, W., "Analysis of the Heat-Shield Experiment on the Pioneer-Venus Entry Probes," AIAA Paper No. 80-1494, July 1980.
[8]Milos, F., et. al, "Analysis of Galileo Probe Heatshield Ablation and Temperature Data," *Journal of Spacecraft and Rockets*, Vol 36, No. 3, June 1999.
[9]Milos, F, et. al, "Mars Pathfinder Entry Temperature Data, Aerothermal Heating, and Heatshield Material Response," *Journal of Spacecraft and Rockets*, Vol. 36, No. 3, May-June 1999.
[10]Santos, J., Oishi, T., Martinez, E., "Isotherm Sensor Calibration Program for Mars Science Laboratory Heat Shield Flight Data Analysis," AIAA Paper No. 2011-3955, June 2011.
[11]Cheatwood, F.M. and Gnoffo, P.A., "User's Manual for Langley Aerothermodynamic Upwind Algorithm (LAURA)," NASA TM-4674, April 1996.
[12]Wright, M. J., Candler, G. V., and Bose, D., "Data-Parallel Line Relaxation Method of the Navier-Stokes Equations," *AIAA Journal*, Vol. 36, No. 9, 1998, pp., 1603-1609.
[13]Mitcheltree, R.A. and P.A. Gnoffo, "Wake Flow About a MESUR Mars Entry Vehicle," AIAA 94-1958, June 1994.
[14]Chima, R., Giel, P., and Boyle, R., "An algebraic turbulence model for three-dimensional viscous flows," AIAA-1993-83, January 1993.
[15]Brown, J.L., "Turbulence Model Validation for Hypersonic Flows," AIAA 2002-3308, June 2002.
[16]Whiting, E.E., Park, C., Liu, Y., Arnold, J.O., and Paterson, J.A., "NEQAIR96, Nonequilibrium and Equilibrium Radiative Transport and Spectra Program: User's Manual," NASA RP-1389, Dec. 1996.
[17]Milos, F.S., Chen, Y.-K. and Squire, T., "Updated Ablation And Thermal Response Program For Spacecraft Heatshield Analysis," Paper TFAWS06-1008, The 17th Thermal and Fluids Analysis Workshop, University of Maryland, August 2006.
[18]Milos, F.S. and Chen, Y-K., "Ablation and Thermal Response Property Model Validation for Phenolic Impregnated Carbon Ablator. AIAA Paper 2009-0262, January 2009
[19]Santos, J., et. al "MISP Error Budget Report," MEDLI Project Internal Document MEDLI-0180, February 2011.
[20]Antill, C., "Sensor Support Electronics Worst-Case Analysis," MEDLI Project Internal Document MEDLI-0114, September 2010.
[21]Hollis, B. R., and Collier, A. S., "Turbulent Aeroheating Testing of Mars Science Laboratory Entry Vehicle in Perfect-Gas Nitrogen," AIAA Paper No. 2007-1208. January 2007.
[22]Beerman, A., et. al, "Development of a Tool to Recreate the Mars Science Laboratory Entry Aerothermal Environment, " AIAA Paper No. 2010-4313, June 2010.
[23]Beck J. V.,et. al, *Inverse Heat Conduction*, John Wiley and Sons, New York, 1985
[24]Mahzari, M., et. al, "An Inverse Parameter Estimation Methodology for the Analysis of Aeroheating and Thermal Protection System Experimental Data" AIAA Paper No. 2011-4027, June 2011.